[Research Paper] 대한금속·재료학회지 (*Korean J. Met. Mater.*), Vol. 57, No. 2 (2019) pp.115-123
DOI: 10.3365/KJMM.2019.57.2.115

Pressure Transmission in the Compaction Process of Nickel Powder Using the Finite Element Methods

Jong Won Baek and Seong Jin Park*

Department of Mechanical Engineering, Pohang University of Science and Technology (POSTECH), Pohang 37673, Republic of Korea

Abstract: The compression process is one of the more widely used industrial manufacturing methods for fabricating desired shape of specimens with various materials such as metals and ceramics. In the compaction process, the upper punch moves into the powder, and force is transmitted between particles, then achieving densification. In this process, the powder can be considered to be in a particulate state, which means that while the powder consists of solids, it has characteristics quite similar to the fluid. Therefore, particles in the process can be seen as responding to hydrostatic pressure, and it can be assumed that the pressure is constant. However, the forces acted on the inter-particle continue to change during the process. Many parameters affect the force change, including compaction speed and the contact angle between particles. However, it is very difficult to verify these effects through experiments because it is impossible to arrange the inter-particle angle. Therefore, in this study, the force transmission mechanism was simulated in the compaction process using FEM simulation. To examine the contact angle and force transmission between the particles, a green compact was modeled as individual particles rather than as a continuum green compact. Finally, it was confirmed through analysis that the pressure transmission between the particles remained constant during the compression process.

(Received December 17, 2018; Accepted December 24, 2018)

Keywords: compaction, FEM simulation, spherical powder, pressure transmission

1. INTRODUCTION

The Powder Metallurgy (PM) process is one of the more widely used methods for manufacturing complex parts in industry. The advantages of this manufacturing technique is that it minimizes material loss and weight [1]. The overall procedure of PM process is as shown in Fig. 1.

The first stage of the PM process is mixing to prepare a compound powder with an additive material such as a lubricant. Before mixing, sieving process is conducted to obtain the desired powder size. Next, a compaction process is carried out to manufacture green compacts with a desired shape. Finally, the green compacts are densified in a sintering stage at high temperature. In the compaction stage, the final pressure (compaction load) is determined, but the force changes continuously during the process. The force change is influenced by the contact angle between the powder and various other conditions. However, it is very hard to determine pressure changes using compaction experiments, because it is impossible to measure the contact angle and contact area. In this case, FEM simulation is a very useful method for examining pressure transmission during the compaction process.

Most prior studies have focused on optimizing the compaction process conditions and geometries to obtain full density [2-10]. Kwon *et al*. [11] and Lee *et al*. [12] carried out simulations on a powder compaction process for complex shapes such as automobile parts, to predict their densities. Also, FEM has been widely used to examine the compaction behavior of metal/ceramic materials [13-18]. However, the powders were considered to be continuum (bulk) green compacts, so particle-particle interaction was not modelled.

The 'particulate state' of matter is peculiar. Powders consist of solid particles yet exhibit fluid-like characteristics.

- 백종원: 박사, 박성진: 교수
**Corresponding Author:* Seong Jin Park
[Tel: +82-54-279-2182, E-mail: sjpark87@postech.ac.kr]

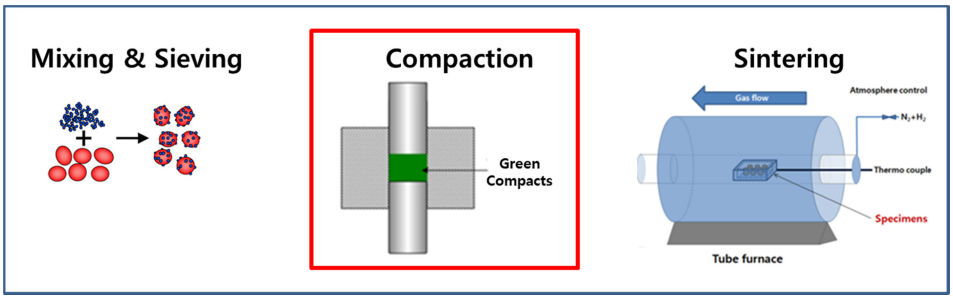

Fig. 1. Overall procedure of PM process

They assume the shape of the vessel into which they are 'poured' and are 'compressible'. The consolidation of powders necessarily involves the transmission of pressure through inter-particle contacts. There are reasons to believe that constrained powders transmit pressure in much the same way that confined liquids do.

When a powder is subjected to isostatic pressing, its linear shrinkage is equal in all directions independent of the particle shape and size distribution. The obtained compact has uniform density throughout its body. During the die-compaction of a powder, the pressure-dependence of densification is close to that obtained during isostatic pressing. In the absence of pressure losses, which are mainly due to die-wall friction, one can expect the pressure-density relation to be independent of the mode of compaction. Even under conditions of unidirectional compaction, the pores retain their shape to a large extent [19]. During sintering, the powder compact undergoes isotropic shrinkage while retaining of its external shape as if it were subjected to isostatic pressing.

Thus, whether pressure is applied externally (compaction) or derived from within (sintering), it can be assumed that a hydrostatic stress state prevails during powder consolidation that is independent of the particle shape and size distribution.

As applied to the compaction of a powder consisting of spherical particles of unequal sizes, Equation (1) reads as follows:

$$P_a = P_{p1} = P_{p2} = \ldots = P_{pn} = l_{p1}/2\pi a_1^2$$

$$= l_{p2}/2\pi a_2^2 = \ldots = l_{pn}/2\pi a_n^2 \quad (1)$$

where P_a is the compaction pressure; P_p is the pressure acting over the surface of a particle of radius a ; and l_p is the total load transferred to the particle [20-23]. If the particles are of the same size, each one of them must carry equal load independent of the number of nearest neighbors (coordination number):

$$P_a = l_p/2\pi a^2 \quad (2)$$

In contrast to liquids, metal powders keep a permanent record of their response to the applied pressure because of their ability to deform plastically. During compaction of a metal powder, each particle attempts to indent its neighbors and, as a result, the inter-particle contacts are converted into contact flats. At a given pressure, the extent of flattening (total contact area) of each particle depends on the inherent resistance of the material of the particles to indentation (hardness) and the total load transferred to it. Thus, measuring the total contact area of the individual particles of a compacted metal powder makes physical verification of equation (1) and (2) possible.

In this study, FEM simulation were conducted to examine the pressure transmission (force transmission) during the compaction process. The nickel particles and cylinder die were modelled by using the ABAQUS 6.13 tool. The simulation results were verified by comparison experimental results. The relationships between particle arrangement angle which affect the contact area, compaction speed, and contact force were obtained.

2. SIMULATION CONDITIONS

Figure 2 shows the initial configuration of the simulation. A total of 9 particles were modeled and located in the cylinder shape die. Vertical speed was applied at the top of the die, while the bottom surface is stationary and rigid.

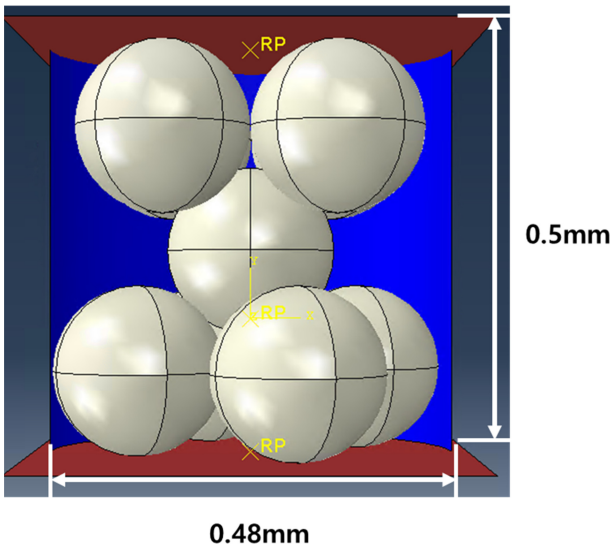

Fig. 2. Initial geometry of the compaction simulation

Table 1. Material properties of slab heater cover parts

Elasticity			Plasticity	
Density (g/cm^3)	Young's modulus (GPa)	Poisson's ratio	Yield stress (MPa)	Plastic strain
7.85	200	0.31	185	0
			290	0.05
			345	0.1
			388	0.15
			413	0.2
			434	0.25

Because it does not move and it is not deformed by the upper punch moving.

The particles were Nickel powder provided by POSCO.

Table 2. Boundary conditions

	Boundary condition		
Bottom	Fix		
Particle arrangement angles	0°, 22.5°, 45°		
Compaction speed	50 mm/s	100 mm/s	200 mm/s

Experiments to investigate mechanical properties of elasticity and plasticity were also carried out and the results are summarized in Table 1.

Also, the boundary conditions were determined as shown in Table 2, to examine the force-displacement relationship and force-contact surface in relation to compaction speed and different particle arrangement angles.

The compaction speed was set to 50, 100, 200 mm/s and the particle arrangement angles were chosen to be 0, 22.5, 45 degrees. Figure 3 demonstrates the modeling of the particle arrangement angles.

In this simulation, the equation of equilibrium was applied as below:

$$\sigma_{ij,j} + f_i = 0 \tag{3}$$

where, σ is a stress, f_i is a body force. Also, stress-strain relationship in elastic (Hooke's law) was determined as below:

$$\sigma = E\varepsilon \tag{4}$$

The plastic strain rate tensor of the metal powder is defined as follows:

$$\dot{\varepsilon}_{ij}^{p} = \lambda \frac{\partial \Phi}{\partial \sigma_{ij}} \tag{5}$$

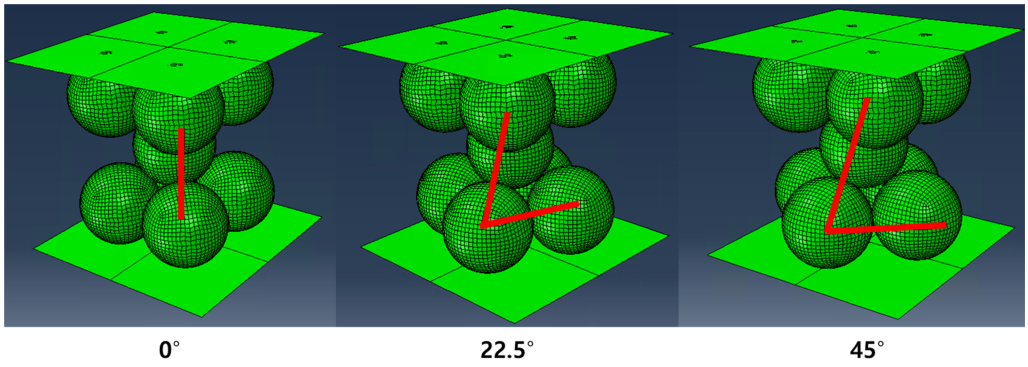

Fig. 3. Particle arrangement angles

where, Φ and $\dot{\lambda}$ are a yield function and the scalar value of the powder material, respectively. The rate of change of the relative density can be written as follows from the mass invariant relation.

$$\dot{D} = -D\dot{\varepsilon}_{kk}^{p} \tag{6}$$

Finally, the plastic yielding behavior of the powder can be defined by the Shima-Oyane equation as follows [24].

$$\Phi(\sigma, \bar{\varepsilon}_{m}^{-p}, D) = \left(\frac{q}{\sigma_m}\right)^2 + 2.49^2(1-D)^{1.028}\left(\frac{p}{\sigma_m}\right)^2 - D^5 = 0 \tag{7}$$

where, q and p are the effective stress and hydrostatic pressure, respectively.

4. RESULTS AND DISCUSSION

4.1. Simulation verification

A compaction experiment was conducted to verify the simulation. The compaction speed was set to 100mm/s with pressure from 20 MPa to 180 MPa increasing in 20 MPa steps (a total 9 data points were obtained). Initially, the particle arrangement degree was 0° to represent the ideal case. Figure 4 shows the initial/final configuration of the simulation. ABAQUS 6.13 was used in this research with an 8-noded solid element, C3D8, with distortion, hourglass mode control. Reduced integration was applied to decrease the computational cost. A total of 102,536 elements were generated with an average aspect ratio of 1.05.

As shown in Fig. 4, the results confirmed that the contact length between the particles or die gradually increased during compaction. A ductile sphere subjected to free-compression under a load l_f undergoes deformation at the points of contact with the flat surfaces forming two circular contacts of equal radius x_f (refer to Fig. 5). The mean contact pressure p_m is given by

$$p_m = l_f/\pi x_f^2 = 2l_f/s_c \tag{8}$$

where $s_c = 2\pi x_f^2$ is the total contact area of the sphere. Note that the mean contact pressure does not depend on the sphere size. Neglecting the deformation-induced increase in the surface area of the sphere, Eq. (8) can be rewritten as

$$l_f = 2\pi a^2 = p_m s_r \tag{9}$$

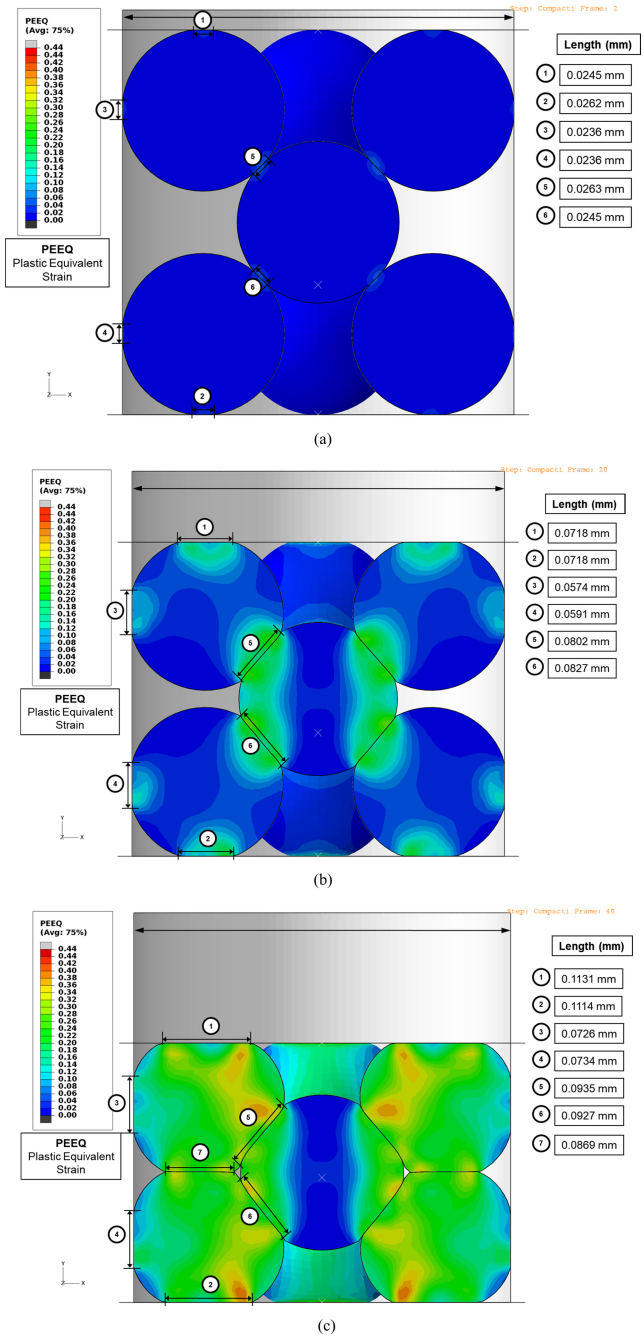

Fig. 4. Compaction simulation at (a) initial configuration, (b) half time configuration, and (c) final configuration

where a is the radius of the sphere; $s_r = s_c/s_o$ is the dimensionless relative contact area of the sphere; and $s_o = 4\pi a^2$ is its original surface area. Equation (9) suggests that the pressure is applied over the surface of the freely compressed sphere $p_f = l_f/2\pi a^2$. Evidently, this pressure-term is independent of the material of the sphere.

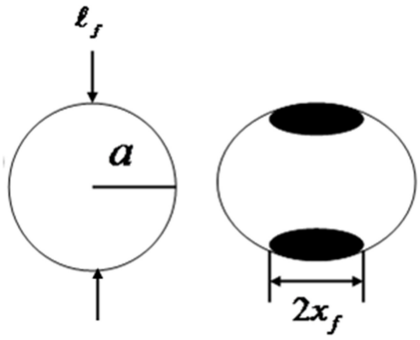

Fig. 5. compression of a ductile sphere

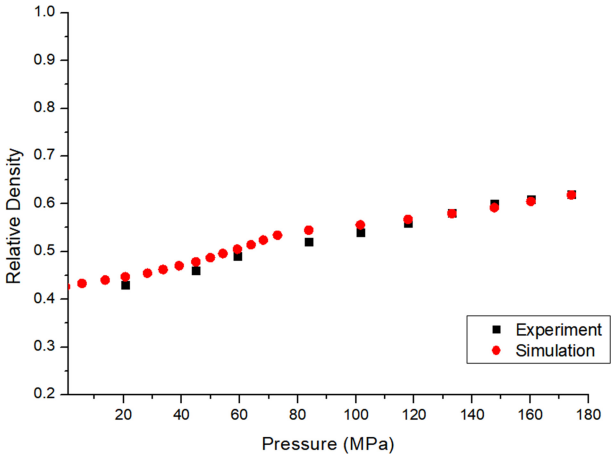

Fig. 6. Pressure-relative density plot for comparing experimental and simulation results

Figure 6 shows the plot of relative density versus pressure for comparison. Comparing the experimental and simulation results (Fig. 6), the maximum error was within 2.5%, and the average error within 1.2%. Therefore, the simulation was verified.

4.2. Force/displacement and contact surface area relationship with different compaction speed

In order to study the effect of compaction speed, simulations were conducted of the force-displacement and force-contact surface area with 0°, 22.5°, and 45° particle arrangement angles. Figure 7 shows the force-displacement relationship with constant angles and different compaction speed.

In 0° and 22.5° case, the force increases almost linearly at 0.11 mm displacement. After that point (0.11 mm), the slope changes abruptly. This is caused by a change in contact area. In other words, the particles at the upper part and lower part were not in contact with each other until the displacement reached 0.11 mm. Therefore, the force increased rapidly. However, as the velocity changed, there was no significant difference observed. Even if the particles contact each other, the rate of increase in contact surface is not sufficiently large [9].

According to the force-contact surface area plot for all cases, force increases linearly at the transition point (inter-particle contact point). After that, force also increases but the gradient changes. Physically, the gradient (slope) is the pressure (force / area) [25-27]. It can be seen that the force is transmitted while the pressure is kept constant, and the compaction process proceeds with constant pressure even after the particles come into contact with each other [28,29]. Also, as the particle rearrangement angle increases, the contact points between the particles gradually move away from the center. Therefore, the point of contact is gradually delayed (the details are shown in Fig. 9).

4.3. Force/displacement and contact surface area relationship with different particle arrangement angles

When the particle arrangement angle is changed, it can be seen that a difference in force is caused by the difference in contact area. Until the particles come into contact with each other, force increases with almost the same slope, but the increase in force after contact is different. Specifically, even though the force transmission among the particles is different with constant pressure applied, pressure was constantly transmitted considering the contact surface area and force. However, the point of force increase was uniqued for each case due to the particle contact angle, as shown in Fig. 9 (a) and (b)

As shown in Fig. 9, when the particle arrangement angle was 22.5 degrees, the powder above contacted one powder located below. However, when the powder was placed at 45 degrees, the powder only contacted 2 particles. This indicates, that when the powder is arranged at 45 degrees, the repulsive force between the powder after contact increases, the pressure increases and the force is transmitted compared to the case of 22.5 degrees. In addition, as shown in Fig. 9

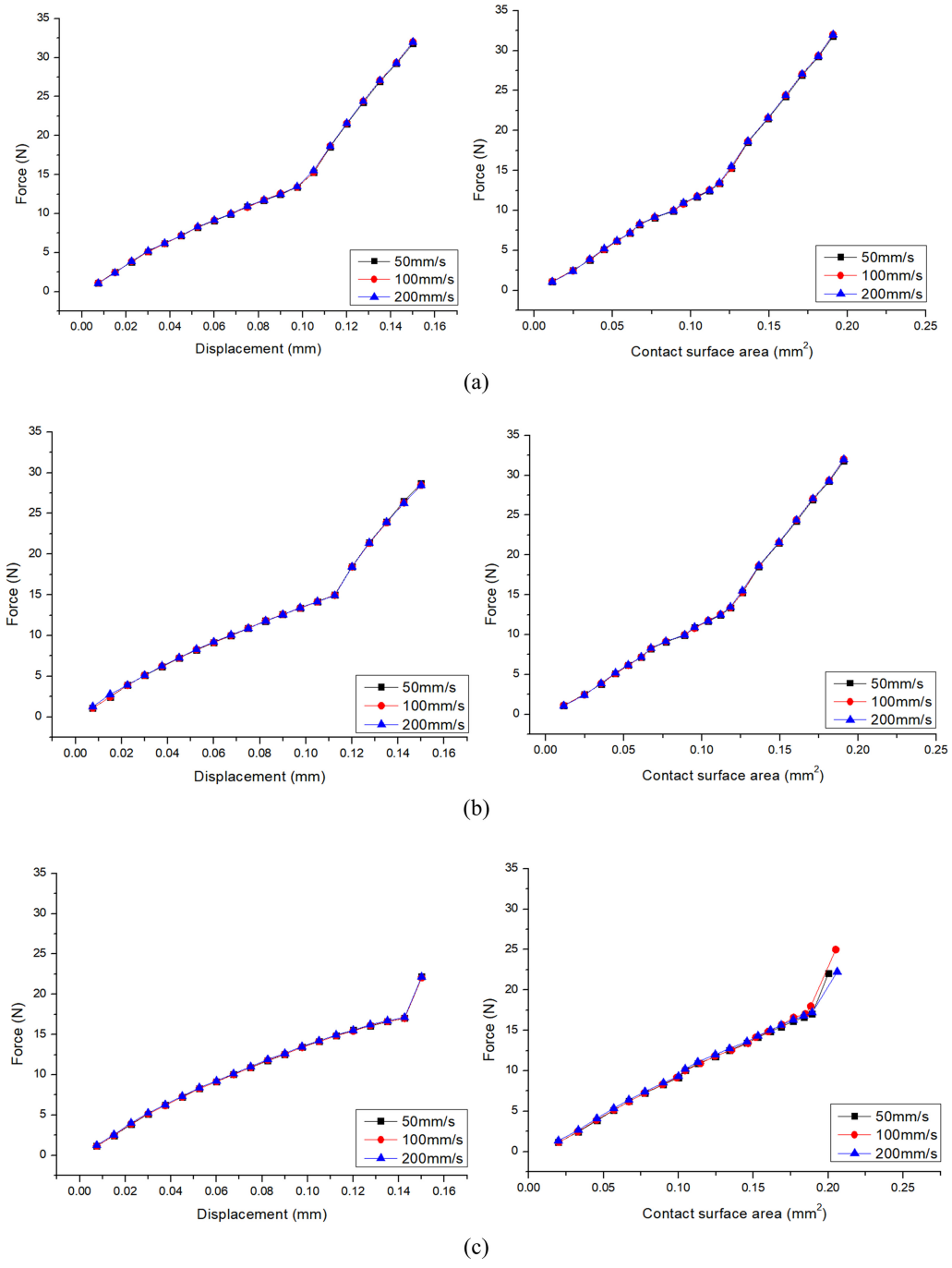

Fig. 7. Force-displacement and force-contact surface area plots with (a) 0°, (b) 22.5°, and (c) 45°

(a), an asymmetry in the contact between the powders appears when they are arranged at 22.5 degrees. This can cause problems, since the powder will be deformed unevenly during the powder compaction process and finally the density distribution will not be uniform.

5. CONCLUSION

An analysis of the pressure transmission phenomenon based on compaction speed and powder arrangement angle was carried out during the powder compaction process. First, to verify the developed analysis program, compressibility curve

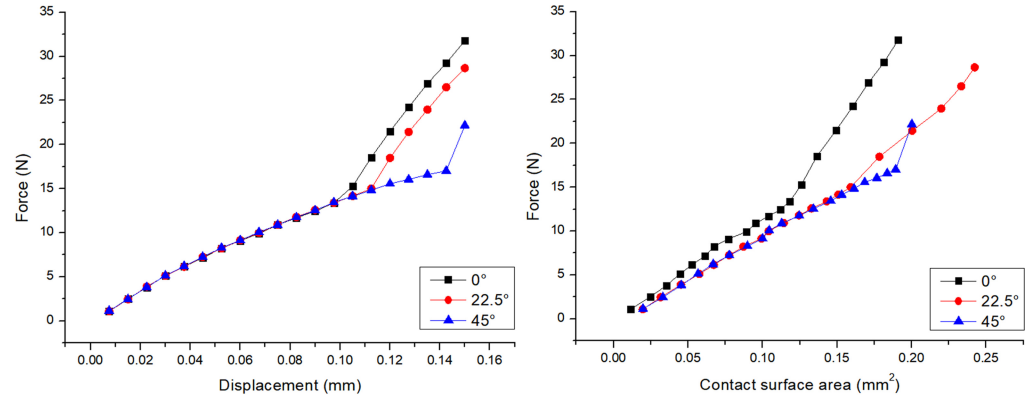

(a)

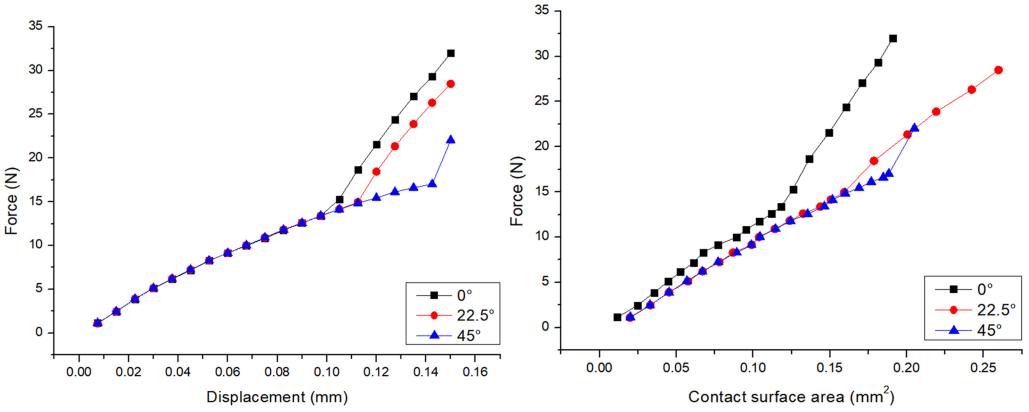

(b)

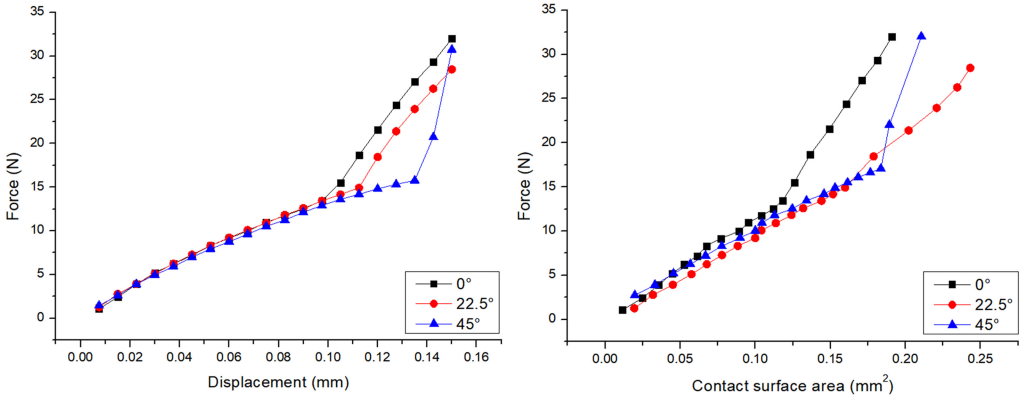

(c)

Fig. 8. Force-displacement and force-contact surface area plots with (a) 50 mm/s, (b) 100 mm/s, and (c) 200 mm/s

were derived through compression process experiments and analyzed under the same condition. As a result, it showed an error of 2.5% or less. The force-displacement, and force-contact area were derived with different compaction speeds. As the compaction speed increased with the same particle arrangement angle, there was no significant difference in the change of force. However, it was confirmed that the point at which the force increases in relation to the particle arrangement angle changes at the same compaction speed. The gradient of all force-contact surface areas remained constant before and after contact. Physically, gradient means pressure in the force-area curve, and the pressure transmission

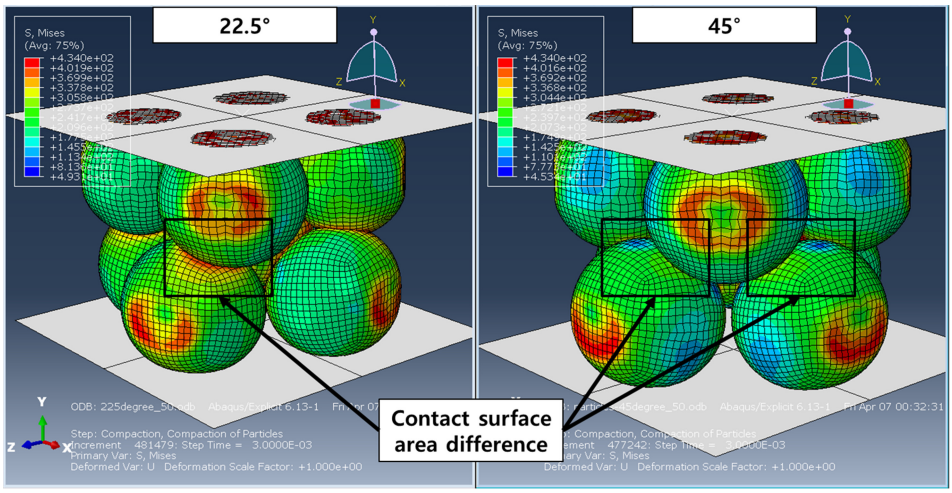

(a)

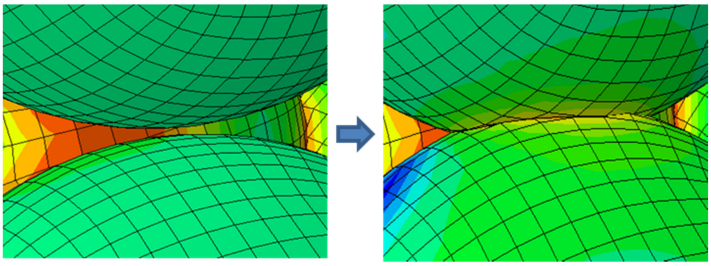

(b)

Fig. 9. (a) Comparing the contact surface area, (b) Particle-to-particle contact point

between particles remains constant as the compaction process progresses. In other words, the force increases, but the contact area also increases accordingly, so it can be seen that the pressure stays constant. The conclusions of this paper are summarized below:

A compaction simulation was conducted at the particle level by using FEM and it determined the relationship between force-displacement / contact surface area.

It was demonstrated that compaction speed, stacking, and the changes occurring in particle coordination during the course of consolidation had no effect on the uniformity of pressure distribution in the powders, and consequently, on the progress of consolidation.

ACKNOWLEDGEMENT

This work was supported by the Industrial Technology Innovation Program(No. 10048358) funded by the Ministry Of Trade, Industry & Energy(MI, Korea)

REFERENCES

1. J. H. Jeong and S. J. Park, *Comp. Mater. Sci.* **100**, 21 (2015).
2. Y. S. Kwon, H. T. Lee, and K. T. Kim, *ASME J. Eng. Mater. Tech.* **199**, 366 (1997).
3. Y. S. Kwon, S. H. Chung, H. I. Sanderow, K. T. Kim, and R. M. German, *Proc. PM2TEC*, *Las Vegas, NV, USA* (2003).
4. A. R. Khoei, A. Shamloo, and A. R. Azami, *Int. J. Solids Struct*. **43**, 5421 (2006).
5. A. R. Khoei, A. R. Azami, and S. Azizil, *J. Mater. Proc. Technol*. **185**, 166 (2007).
6. A. R. Khoei, M. Anahid, and K. Shahim, *J. Mater. Proc. Technol*. **185**, 397 (2007).
7. R. Rossi, M. K. Alves, and H. A. Al-Qureshi, *J. Mater. Proc. Technol*. **182**, 286 (2007).
8. S. C. Lee and K. T. Kim, *Mater. Sci. Eng. A* **445**, 163 (2007).

9. C. Y. Wu, B. C. Hancock, A. Mills, A. C. Bentham, S. M. Best, and J. A. Elliott, *Powder Technol.* **181**, 121 (2008).
10. S. C. Lee and K. T. Kim, *Int. J. Mech. Sci*. **44**, 1295 (2002).
11. Y. S. Kwon, S. H. Chung, K. T. Kim, R. M. German, and H. I. Sanderow, *Adv. Powder Metall. Part. Mater.* **4**, 4 (2003).
12. M. C. Lee, *Powder Metall*. **51**, 1 (2008).
13. B. J. Briscoe and S. L. Rough, *Colloid. Surface. A* **89**, 103 (1996).
14. I. Aydin, B. J. Briscoe, and N. Ozkan, *MRS Bulletin* **22**, 45 (1997).
15. PM MODNET Research Group, *Powder Metall.* **45**, 335 (2002).
16. PM MODNET Computer Modelling Group, *Powder Metall.* **42**, 301 (1999).
17. O. Coube and H. Riedel, *Powder Metall.* **43**, 123 (2000).
18. L. N. Smith, *Powder Metall.* **45**, 294 (2002).
19. H. F. Fischmeister, E. Arzt, and L. R. Olsson, *Powder Metall.* **21**, 179 (1973).
20. J. V. Kumar, *Sintered Metal-Ceramic Composites* (1984).
21. J. V. Kumar, *Technical Report No. MDN 10 1987, Mishra Dhatu Nigam Limited* (1987).
22. J. V. Kumar, *Solid State Phenom.* **8**, 125 (1990) .
23. J. V. Kumar and C. S. Kumar, *Adv. Powder Metall. Part. Mater.* **2**, 5 (1995).
24. S. Shima, Y. Sakamoto, and H. Kotera, *Int. J. Mech. Sci*. **44**, 1603 (2002).
25. S. V. Atre, S. J. Park, R. Zauner, and R. M. German, *Powder Metall.* **50**, 1 (2007).
26. S. H. Chung, Y. S. Kwon, S. J. Park, and R. M. German, *Finite Element in Analysis and Design* **45**, 11 (2009).
27. L. A. Jaeckel, *The Annals of Mathematical Statistics* (1972).
28. J.-H. Lee, S. J. Park, J. Moon, J.-Y. Kang, J. Y. Park, T.-H. Lee, and K. M. Cho, *Korean J. Met. Mater.* **55**, 363 (2017).
29. J. Y. Park, S. J. Park, J. H. Lee, J. Moon, T. H. Lee, K. J. Jeong, and J. H. Shin, *Korean J. Met. Mater.* **55**, 12 (2017).
30. G. Rubio, N. Agrait, and S. Vieira, *Phys. Rev. Lett*. **76**, 2302 (1996).
31. S. Dubois, L. Piraux, J. M. Gerge, K. Ounadjela, J. L. Duvail, and A. Fert, *Phys. Rev. B* **60**, 477 (1999).
32. M. F. Horstemeyer and D. J. Bammann, *Int. J. Plast.* **26**, 1310 (2010).
33. D. N. Lee and H. S. Kim, *Powder Metall.* **35**, 275 (1992).